sustainability

MDPI

Article

Analysing the Performance of Four Hydrological Models in a Chinese Arid and Semi-Arid Catchment

Hengxu Jin [1], Xiaoping Rui [2,*] and Xiaoyan Li [1]

[1] School of Geomatics, Liaoning Technical University, Fuxin 123000, China; jin960707@163.com (H.J.); 472120757@stu.lntu.edu.cn (X.L.)
[2] College of Earth and Engineering, Hohai University, Nanjing 211100, China
* Correspondence: ruixp@hhu.edu.cn

Abstract: Frequent flood hazards in the Raoyang River Basin in western Liaoning, China, have posed serious threats to people's lives and property. In an effort to study the simulation efficiencies of hydrological models in this arid and semi-arid catchment, this study examined the performance of the Xin'anjiang model, the Liaoning unsaturated model, and the DHF model in the Dongbaichengzi station watershed in the upper reaches of the Raoyang River, China. Additionally, this paper proposed an improved DHF model, which considers the impoundment and regulation of small- and medium-sized reservoirs in the upper reaches of the basin. The flood simulation results demonstrated that the Xin'anjiang model was difficult to apply in this area because the average value of its Nash–Sutcliffe efficiency (NSE) was as low as 0.31. Meanwhile, the simulation efficiencies of the Liaoning unsaturated model and the DHF model were higher than that of the Xin'anjiang model, but the relative error of flood peak discharge and runoff depth for most floods were still high and could not meet the actual forecast requirements by the Reservoir Administration Bureau of Liaoning Province. Overall, the improved DHF model showed the best efficiency, and the mean value of the NSE reached 0.79. Therefore, the improved DHF model has good applicability in the Dongbaichengzi station watershed in the upper reaches of the Raoyang River, China.

Keywords: arid and semi-arid regions; flood forecasting; DHF model; impact of small and medium-sized reservoirs; Raoyang River basin in western Liaoning

Citation: Jin, H.; Rui, X.; Li, X. Analysing the Performance of Four Hydrological Models in a Chinese Arid and Semi-Arid Catchment. *Sustainability* **2022**, *14*, 3677. https://doi.org/10.3390/su14063677

Academic Editors: Aristeidis Kastridis and Dimitrios Stathis

Received: 16 February 2022
Accepted: 18 March 2022
Published: 21 March 2022

1. Introduction

The risk of flooding is expected to rise in the 21st century due to the anthropogenic environment and the increasing frequency of extreme precipitation events resulting from climate change [1–3]. Many severe flood events have been reported across the world in the last two decades [4], for example, New York City, USA, in October 2012, Uttarakhand, India, in July 2013, Western Japan in July 2018, Northern Queensland, Australia, in February 2019, Dhaka, Bangladesh, in July 2020 and Zhengzhou, China, in July 2021 [5–8]. Floods are the most frequent type of natural disasters and pose a huge threat to society [9,10]. Hydrological forecasting plays an effective role in flood prevention and disaster reduction [11–14]. While most hydrological models work well in humid areas with frequent floods [15–18], these models exhibit poor simulation results in arid and semi-arid areas [19,20].

Several reasons explain the poor simulation efficiencies of hydrological models in arid and semi-arid areas [21–23], including the following: (1) rainfall and runoff in such areas often display a strongly nonlinear relationship, and most hydrological models have difficulties describing the complex runoff mechanisms in these areas [24,25]; (2) the soil water content in this basin is low, making it less likely to be filled by rainfall [26–29]; (3) in the absence of rain for an extended period, anthropogenic factors such as the small- and medium-sized reservoirs in the upper reaches of the basin have less water in storage, and the impact of rainfall is greatly affected by the impoundment of such reservoirs, resulting

in large flood-forecast errors [30,31]. Several studies contributed to the improvement of hydrological models in arid and semi-arid regions [32]. For example, Bao et al. [33] and Luo et al. [34] proposed a vertical mixing model and an interactive model, respectively. These two models considered runoff yield under excess infiltration and runoff yield under excess saturation. Jin et al. [35] proved that the Soil Conservation Service curve number (SCS-CN) model demonstrated a relatively good result for situations with short rainfall duration but high intensity in the Jianghe watershed, which is located in a semi-arid area of Northern China. A method based on coupling discrete wavelet transforms (WA) and artificial neural networks (ANN) for flow forecasting applications in nonperennial rivers was proposed by Adamowski et al. [36], who showed that coupled wavelet neural network models were a promising new method of short-term flow forecasting in nonperennial rivers in semi-arid watersheds. Sharifi Garmdareh et al. [37] compared the support vector regression (SVR) model with the adaptive neuro-fuzzy inference system (ANFIS), artificial neural network (ANN), and nonlinear regression (NLR) models in the regional flood frequency analysis (RFFA) of the Namak Lake watershed. The results showed that the gamma test (GT) technique improved the models' performance in arid and semi-arid regions of Iran. Overall, even though the simulation efficiencies of hydrological models in arid and semi-arid regions has been improved to some extent [38–40], it is difficult to apply these models in the Raoyang River Basin because few studies have taken into account the arid and semi-arid environment and the impact of reservoirs [41–44] for hydrological modelling in this catchment.

To study the simulation efficiencies of hydrological models in the Raoyang River Basin in western Liaoning, China, we selected the most widely used Xin'anjiang model, the Liaoning unsaturated model proposed by the Hydrology Bureau of Liaoning Province, China, the DHF model, and the improved DHF model. The aims of this study are summarized as follows:

(1) To study the impoundment and regulation effect of small- and medium-sized reservoirs in the upper reaches of the research basin, an improved DHF model was proposed. This model quantifies the impoundment effect of upstream reservoirs by calculating the prewater storage volume and the reservoir cut-off. In order to calculate the regulation effect of reservoirs in the upper reaches of the basin, this paper considers the spatial distribution of rainfall in the basin, the cumulative rainfall and the soil moisture content.

(2) To study the simulation efficiencies of hydrological models in this arid and semi-arid catchment, this study examined the performance of the Xin'anjiang model, the Liaoning unsaturated model, the DHF model, and the improved DHF model in the Dongbaichengzi station watershed in the upper reaches of the Raoyang River, China.

The rest of paper was organized as follows: In Section 2, a description of the research catchment and data sources is provided; additionally, the widely-used Xin'anjiang model, the Liaoning unsaturated model, the DHF model, and the improved DHF model are introduced. In Section 3, the improved DHF model and the other three models are calibrated for the study catchment, and the simulation results of the four models are compared and discussed. Section 4 provides a summary and additional discussion on the limitations and future directions for improvements.

2. Materials and Methods

2.1. Study Area

We focused on the Dongbaichengzi station watershed in the upper reaches of the Raoyang River. The watershed area is 2138 km^2. The land in the basin is barren, and the soil erosion is severe. According to the flood database of Liaoning Province, the most notable floods in the past 100 years occurred in 1953, 1962, 1969, 1975, 1984, and 2013 [45]. The annual precipitation in the basin is 455–530 mm, and summer precipitation accounts for more than 75% of the yearly accumulation. This arid and semi-arid area often experiences torrential rain and short durations of confluence after a long drought, which make forecasting more difficult [46]. The study focused on the Dongbaichengzi station

watershed in the upper reaches of the Raoyang River, calibrating each model according to the data of upstream small- and medium-sized reservoirs, soil moisture content, and other available data. Figure 1 illustrates the river network of the Dongbaichengzi watershed, while Table 1 presents characteristics for the small- and medium-sized reservoirs in the upper reaches of the Raoyang River.

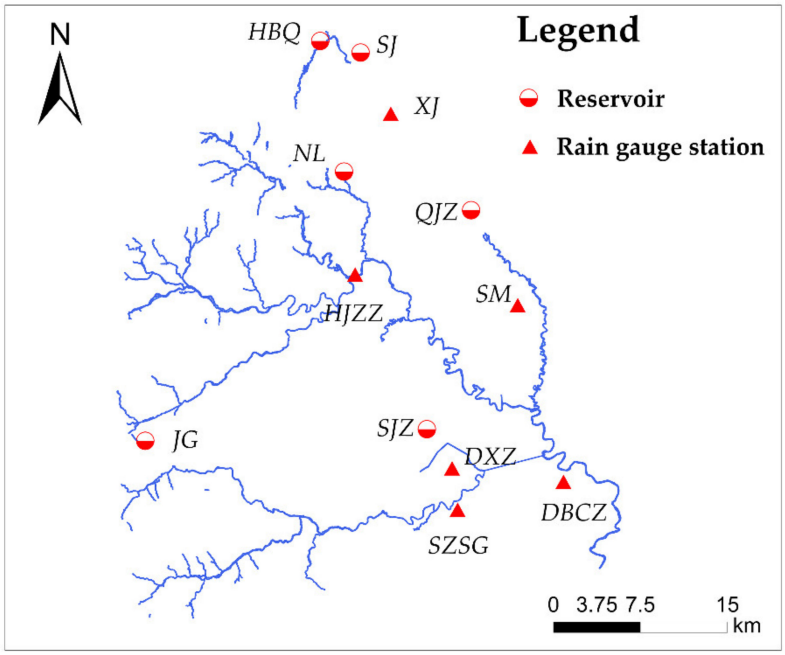

Figure 1. Map of the Dongbaichengzi station watershed in the upper reaches of the Raoyang River.

Table 1. Characteristics of the reservoirs located in the upper reaches of the Raoyang River.

Station Code	Name	Type	River Name	Reservoir Capacity (km^3)	Above Sea Level (m)	
					Flood Control Water Level	Design Low Water Level [47]
21010320	Jianguo (JG)	Medium	Wuhuanchi	12,050	182.42	176.64
21010625	Sanjiazi (SJZ)	Small	Erdaohe	7280	158.50	154.89
21011120	Habaqin (HBQ)	Small	Weitang	4080	44.60	44.40
21200330	Qijiazi (QJZ)	Small	Weitang	8500	148.00	145.20
21010820	Shijia (SJ)	Small	Shijiahe	1300	48.50	44.14
21011320	Nanliu (NL)	Small	Raoyang	1000	44.40	43.24

2.2. Hydrological Data

This paper uses the rain and flood data from 1955 to 2013 from the Liaoning Hydrological Yearbook [48]. The rainfall data are from six main rain gauge stations: Hanjiazhangzi (HJZZ), Shuangmiao (SM), Shangzhaoshugou (SZSG), Dongbaichengzi (DBCZ), Daxingzhuang (DXZ), and Xujia (XJ). The rain gauge station data include the starting time of the rainfall, the time to reach the rainfall peak, and the historical precipitation. The measured data for the hydrological station include data such as the start time of the flood, the time to reach the flood peak, and the historical discharge. This paper lists 13 floods, 9 of which were used for model calibration, while the remaining 4 were used for model validation [48].

2.3. Xin'anjiang Model

The Xin'anjiang model was proposed in 1973 to enable Xin'anjiang reservoir inflow forecasting [49,50]. The generated runoff is separated into three components, which includes surface runoff, interflow, and groundwater. The Xin'anjiang model is based on the watershed saturation–excess runoff theory, which asserts that the runoff-generation

processes usually occur in humid and semi-humid regions. The Xin'anjiang model neglects the processes of plant interception, filling depressions, evaporation, and infiltration in the calculation. The formula for the water storage capacity curve in the runoff calculation of this model is as follows:

$$\delta = 1 - \left(1 - \frac{WM}{MWM}\right)^{\lambda} \tag{1}$$

where δ is a ratio of the runoff-generation area to the total basin area, λ is the exponent of the curve which needs to be calibrated in modelling, WM and MWM are the water storage capacity and its maximum value for the soil in the basin, respectively. In the confluence calculation model, the linear reservoir algorithm is used to calculate the groundwater runoff and subsurface flow. Detailed descriptions of the principles behind the Xin'anjiang model can be found in the relevant literature [51–53].

2.4. Liaoning Unsaturated Model

The Liaoning unsaturated model is mainly used in the western Liaoning province, China. The runoff of this model is controlled by the infiltration capacity of the watershed [54]. Runoff occurs when the instantaneous infiltration rate f is less than the rainfall intensity i. The runoff depth R in period Δt can be described as

$$R = \Delta t(i - f) \tag{2}$$

The Horton formula is used to reflect the change of surface infiltration capacity, as follows:

$$f = f0e^{-\beta t} + fc\left(1 - e^{-\beta t}\right) \tag{3}$$

where f, $f0$, and fc are the instantaneous infiltration rate, the initial infiltration rate, and the stable infiltration rate, respectively (all units are mm/h), while β is an empirical exponent, and its value is 0.5 [54]. For the sake of practicality, let Δt be the length of the time period. Through integral calculation, the average infiltration rate $\overline{f}$ is obtained using the following formula:

$$\overline{f} = \int_{t}^{t+\Delta t} [fc + (f0 - fc)e^{-\beta t}]dt = (\frac{1 - e^{-\beta \Delta t}}{\Delta t})(Im - Pa) + [1 - \frac{Im - Pa}{\beta Im}(\frac{1 - e^{-\beta \Delta t}}{\Delta t})]fc \tag{4}$$

where Im is the maximum water storage capacity and Pa is the observed water storage capacity.

The infiltration rate of each point in the watershed is different at different times and in different spaces. This phenomenon led to proposal of the concept of $\overline{f}$'s spatial distribution [54]. In other words, a method based on the unit area of the watershed is used to solve the problem of uneven distribution of rainfall intensity. So, the formula for the area of runoff yield is

$$\frac{F_0}{F} = 1 - e^{-af} \tag{5}$$

where F_0 is the area of runoff yield, F is the area of the entire watershed, and α represents a parameter that reflects the distribution characteristics of the average infiltration rate.

Let the average rainfall intensity be $i0$, then the average runoff depth per unit time $R0$ is

$$R0 = \int_{0}^{i0} (1 - e^{-af})df = i0 - \frac{1}{a}(1 - e^{-ai0}) \tag{6}$$

where $R0$ is the average runoff depth per unit time, f is the infiltration rate, $\overline{f}$ is the average infiltration rate, and α represents a parameter that reflects the distribution characteristics of the average infiltration rate.

When $i0 = \infty$, the average runoff depth per unit time $R0$ is

$$R0 = i0 - \overline{f}(1 - e^{-\frac{i0}{\overline{f}}}) \tag{7}$$

So, the formula for the runoff depth in period Δt is

$$R = R0\Delta t = (i0 - \overline{f})\Delta t = \Delta P - \overline{f}\Delta t \quad (8)$$

where ΔP is the rainfall during that period (expressed in mm as the unit).

2.5. DHF Model

In the 1970s, the DHF Reservoir Administration Bureau of Liaoning Province proposed the DHF rainfall-runoff model (DHF) for the arid and semi-arid areas in Northern China, and this model has been widely used in certain northern river basins in recent years. The model consists of two parts: (1) the confluence calculation model with variable speed and variable strength and (2) the hyperosmosis runoff calculation model, which describes the distribution of the lower infiltration rate and surface water storage with a parabolic function and is calculated using the double-layer infiltration curve. Figure 2 illustrates the structure of the model. The meanings of the variables in the figure are as follows: P and P_E are the rainfall and net rainfall intensity, respectively; R, R_C, and R_L are the infiltration intensity, the infiltration intensity of the lower layer, and the percolation rate of the groundwater, respectively; S_0, U_0, and V_0 are the maximum value of the surface water storage capacity, the maximum value of the lower layer water storage capacity, and the maximum value of the groundwater storage capacity, respectively; U_a and V_a represent the underlying soil water storage and groundwater storage, respectively; E_D is the evaporation between rainfall events; y_0 is the runoff from the impervious area; g is the proportion of the impervious area to the total watershed area; f is the average infiltration rate of the entire watershed; and K_W is the groundwater runoff scaling factor [55]. The particle swarm optimisation algorithm [56–58], which was widely used in the hydrological model, was used to calibrate the model's parameters.

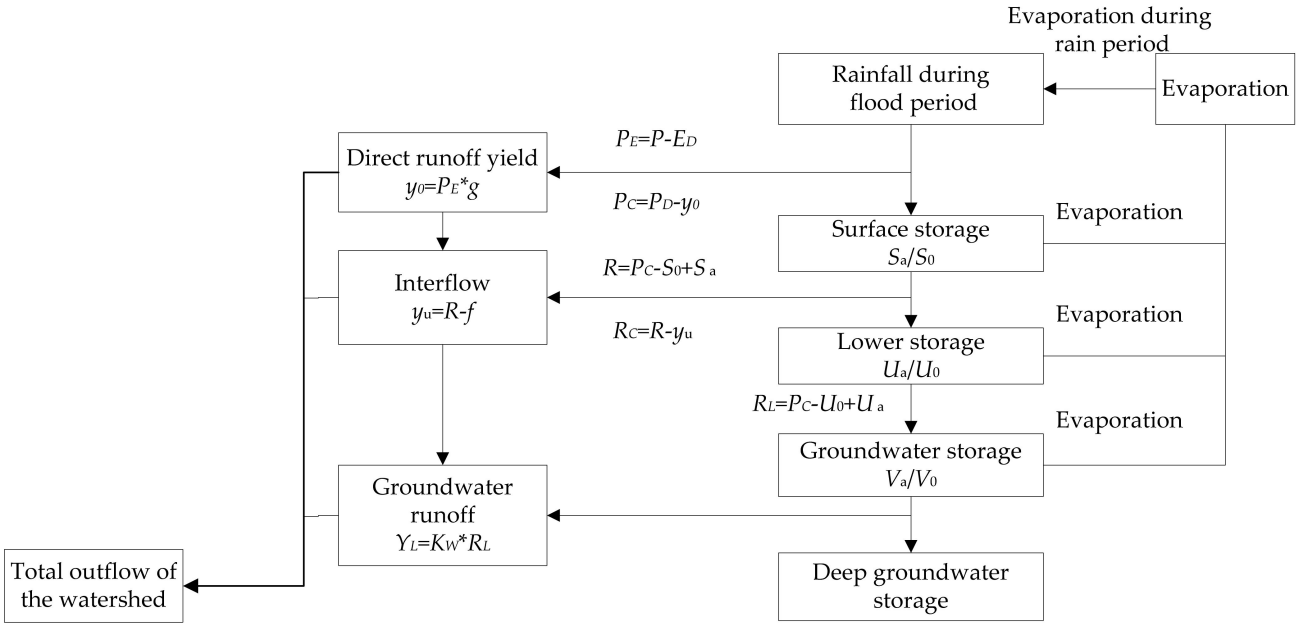

Figure 2. Structure of DHF model.

2.6. Improved DHF Model

In arid and semi-arid regions where there is no rainfall for long stretches of time, the reservoirs in the upper reaches of the basin lack water storage in the early stage of a rainfall event. Thus, such reservoirs will intercept a large portion of rainfall, affecting the runoff yield and confluence of the basin. In view of this phenomenon, we improved the original DHF model in Section 2.5. This enhanced structure is shown in Figure 3 (the solid-line frames denote the proposed changes).

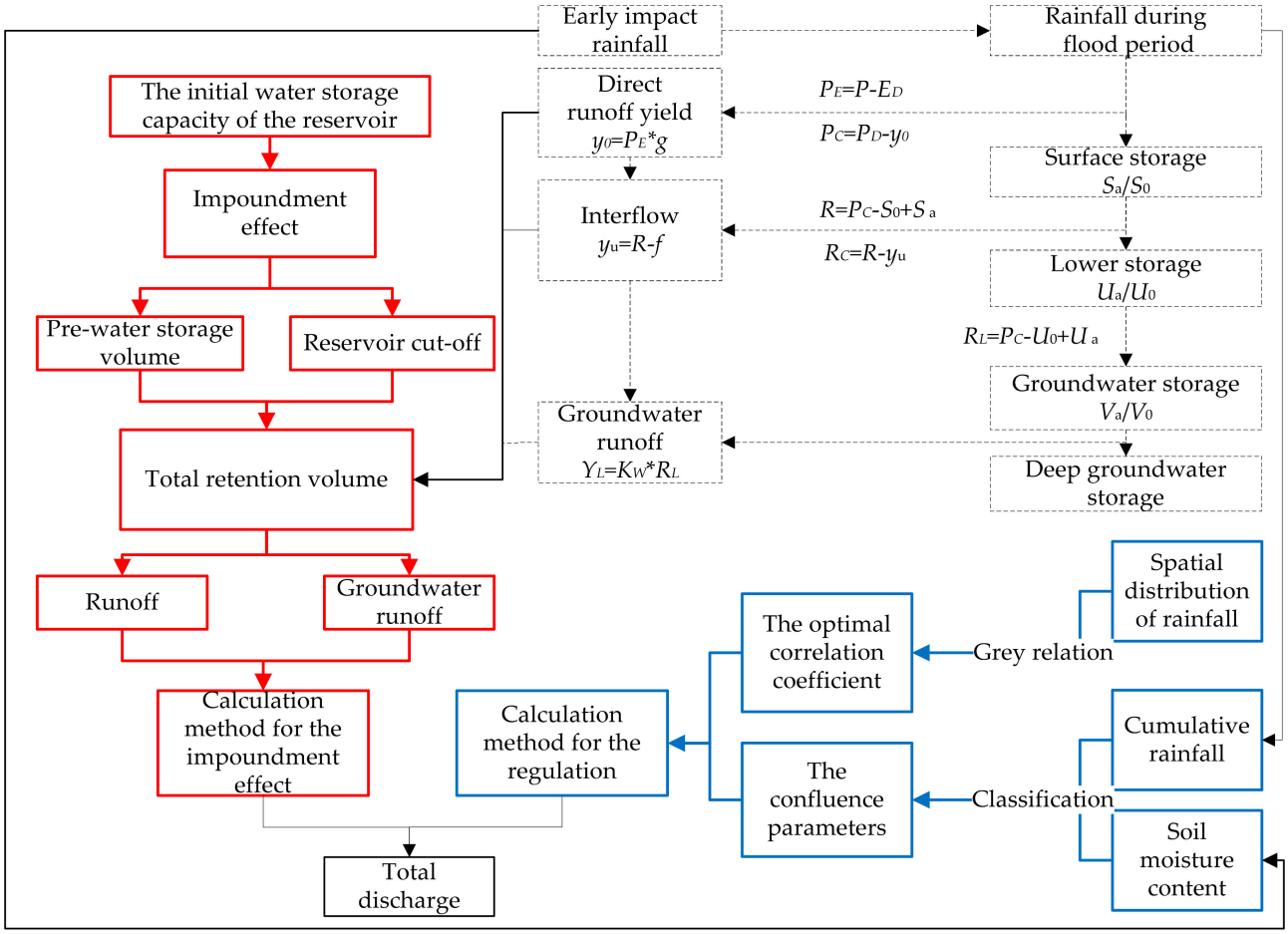

Figure 3. Structure of the improved DHF model considering the influence of upstream reservoirs.

The meaning of the variables in Figure 3 is the same as in the original DHF model in Section 2.5. The improved model considers the impoundment and regulation effect of small- and medium-sized reservoirs in the upper reaches of the research basin. Specifically, as shown in the parts marked in red in Figure 3, the impoundment effect is calculated by the water balance; as shown in the parts marked in blue in Figure 3, we considered the spatial distribution of rainfall in the basin, the cumulative rainfall, and the soil moisture content when calculating the regulation effect of upstream small- and medium-sized reservoirs. The following is a brief description of the two parts of the proposed changes.

2.6.1. Calculation Method for the Impoundment Effect of Small- and Medium-Sized Upstream Reservoirs

We quantified the impoundment effect of upstream reservoirs by calculating the prewater storage volume and the reservoir cut-off. The formula for calculating the prewater storage volume of the reservoir V_0 is

$$V_0 = V_X W_0/(W_1 + W_2) \tag{9}$$

where V_X is the storage capacity of the reservoir, W_0 is the initial water content of the soil, and W_1 and W_2 are the water storage capacity of the upper and lower soil layers of the basin, respectively. The storage volume $V_i(t)$ of each reservoir and the total retention volume $W(t)$ of the reservoir according to the water balance are calculated using the following formula:

$$V_i(t) = \begin{cases} i(t)S_i + V_i(t-1) & V_i(t-1) < V_{iX} \\ 0 & V_i(t-1) \geqslant V_{iX} \end{cases} \tag{10}$$

$$W(t) = \sum_{n}^{i=1}(V_i(t) - V_i(t-1)) \tag{11}$$

where n is the number of reservoirs in the study area, $V_i(t)$ is the water storage capacity of the reservoir i at time t, $i(t)$ is the net rainfall at time t, and S_i and V_{iX} are the catchment area of the reservoir i and beneficial reservoir capacity, respectively. According to Formulas (10) and (11), the runoff depth and retention depth of the reservoir during each period of the flood can be calculated, facilitating the calculation for the impoundment of small- and medium-sized upstream reservoirs.

2.6.2. Calculation Method for the Regulation of Upstream Small- and Medium-Sized Reservoirs

Since the upstream reservoirs change the confluence time and area of a flood, we considered the spatial distribution of rainfall in the basin, the cumulative rainfall, and the soil moisture content when calculating the regulation effect of upstream small- and medium-sized reservoirs:

(1) The uneven spatial distribution of rainfall will inevitably affect the confluence of the upstream reservoirs. In view of this fact, we adopted the grey relation analysis model [59]. According to the measured hydrological data of the basin over the years, the grey relation analysis can be used to calculate the correlation coefficient between each amount from a rain gauge station (the rainfall data are from six main rain gauge stations) and the total basin discharge. In addition, this paper analyses the influence of the uneven spatial distribution of rainfall on the fluctuation of the total basin discharge. Next, the multiple linear regression model [60] is used to validate the flood discharge and calculate the optimal correlation coefficient of each rain gauge station.

First, a data matrix is formed by setting a parent sequence $x_0(t)$ and several subsequences $x_i(t)$:

$$z = \begin{Bmatrix} x_0(1) & \cdots & x_n(1) \\ \vdots & \cdots & \vdots \\ x_0(t) & \cdots & x_n(t) \end{Bmatrix} \tag{12}$$

where $x_i(t)(i = 1, 2 \ldots n)$ represents the independent variable (influencing factor) in the analysis data (amount of rainfall at each rain gauge station) and $x_0(t)$ represents the dependent variable in the analysis data (total basin discharge). To solve the problem of the unit of the parent sequence and the subsequence being different, the newly formed expression of the parent sequence $x'_0(t)$ and the subsequence $x'_i(t)$ is calculated as follows:

$$x'_0(t) = \frac{x_0(t)}{x_0(1)}, x'_i(t) = \frac{x_i(t)}{x_i(1)} \tag{13}$$

Then, the absolute difference $\Delta_{0i}(t)$ between the parent sequence $x'_0(t)$ and the subsequence $x'_i(t)$ is calculated using Formula (14) to form the different sequence for each factor. Substituting the maximum values Δ_{min} and Δ_{max} in the absolute value matrix into Formula (15) facilitates calculating the correlation coefficient $\delta_{0i}(t)$ between the parent sequence and the subsequence:

$$\Delta_{0i}(t) = \left|x'_0(t) - x'_i(t)\right|, i = 1, 2 \cdots n \tag{14}$$

$$\delta_{0i}(t) = \frac{\Delta_{\min} + k\Delta_{\max}}{\Delta_{0i}(t) + k\Delta_{\max}}, i = 1, 2 \cdots n \tag{15}$$

where t represents the time, i represents the influencing factor in the watershed, n is the number of influencing factors in the watershed, and k represents the resolution ratio, generally between 0 and 1 [59].

Finally, according to Formula (16), the relational degree ζ_{0i} of each influencing factor (each amount of a rain gauge station) in the watershed is calculated as follows:

$$\zeta_{0i} = \frac{1}{n}\sum_{i=1}^{n}\delta_{0i}(t) \tag{16}$$

where n is the number of influencing factors which represents the number of rain gauge stations in the watershed.

(2) To fully consider the effect of cumulative rainfall over time on the regulation of small- and medium-sized reservoirs in terms of floods and downstream confluence, we calculated the cumulative rainfall in each simulated event and divided it into eight rainfall levels: the first level is the steady infiltration amount, and the second level starts to gradually increase in steps of 20 mm. Iteratively, the rainfall level is divided, as shown in Table 2.

Table 2. Rainfall classification table. (Taking the stable infiltration volume γ = 5 mm in the watershed as an example.)

Rainfall Level	**1**	**2**	**.....**	**7**	**8**
Infiltration amount\mm	[0, 5]	(5, 25]	.....	(105, 125]	(125, +∞)

In arid and semi-arid regions, the initial storage capacity of small- and medium-sized reservoirs will vary with soil moisture content, which leads to the regulation of runoff yield by small- and medium-sized reservoirs. Moreover, the water content of the soil also has a large impact on the confluence mechanism. The model divides floods into four categories—moist, semi-moist, semi-arid, and arid—and then takes them into account with the rainfall level to determine *DD* (a confluence parameter that reflects flood peak discharge) and *CC* (a confluence parameter that reflects flood peak time) [55] according to the degree of soil moisture. Taking the stable infiltration volume γ = 5 mm in the watershed as an example, Table 3 displays the optimal results of the confluence parameters.

Table 3. Optimal results of confluence parameters.

		Rainfall Level							
Soil Moisture	***DD***	**1**	**2**	**3**	**4**	**5**	**6**	**7**	**8**
					CC				
Moist	0.70	1.0	2.3	2.9	0.7	0.5	2.7	0.9	3.6
Semi-moist	0.70	2.0	2.6	2.5	1.1	3.9	2.2	2.6	3.3
Semi-arid	1.05	2.7	2.1	2.2	1.4	3.7	2.0	3.0	2.2
Arid	1.15	3.2	0.9	1.9	1.6	3.0	3.4	3.3	0.5

2.7. Efficiency Measures

In this paper, the error of flood peak time E_1, the relative error of flood peak discharge E_2, the relative error of runoff depth E_3, and the NSE were selected as efficiency measures [61]. We used these four indicators to compare the simulation efficiencies of the different models. The closer E_1, E_2, and E_3 were to 0, and the closer NSE was to 1, the better the simulation efficiency. An NSE value greater than 0.75 represents good performance of the model [62]. The calculation formulas are as follows:

$$E_1 = \left|T_{p,s} - T_{p,o}\right| \tag{17}$$

$$E_2 = \left|\frac{Q_{p,s} - Q_{p,o}}{Q_{p,o}}\right| \times 100\% \tag{18}$$

$$E_3 = |\frac{R_s - R_o}{R_o}| \times 100\% \quad (19)$$

$$NSE = 1 - \frac{\sum_{i=1}^{n} (Q_{p,s,t} - Q_{p,o,t})^2}{\sum_{i=1}^{n} (Q_{p,o,t} - Q_o)^2} \quad (20)$$

where $T_{p,o}$ is the observed flood peak time, $T_{p,s}$ is the simulated flood peak time, $Q_{p,o}$ is the observed flood peak discharge, $Q_{p,s}$ is the simulated flood peak discharge, R_o is the observed runoff, R_s is the simulated runoff, $Q_{p,o,t}$ is the observed instantaneous discharge, $Q_{p,s,t}$ is the simulated instantaneous discharge, and Q_o is the average measured discharge.

3. Results and Discussion

3.1. Flood Simulation Results

Table 4 shows the simulation efficiencies for all flood event simulations (both calibration and validation periods) by using the Xin'anjiang model, the Liaoning unsaturated model, the DHF model, and the improved DHF model.

Table 4. Flood simulation results (X, L, D, and I represent the Xin'anjiang model, the Liaoning unsaturated model, the DHF model, and the improved DHF model, respectively).

Year		Error of Flood Peak Time/h				Relative Error of Flood Peak Discharge/%				Relative Error of Runoff Depth/%				Nash–Sutcliffe Efficiency			
		X	L	D	I	X	L	D	I	X	L	D	I	X	L	D	I
Calibration	1962	4	1	4	1	41.8	50.1	35.1	18.1	66.8	45.5	12.6	2.6	0.52	0.64	0.71	0.85
	1963	4	1	4	2	56.7	37.5	25.4	10.4	8.6	6.7	16.0	36.0	0.44	0.67	0.68	0.75
	1964	6	0	2	1	28.0	18.1	36.2	16.8	18.8	31.7	30.2	10.1	0.53	0.79	0.78	0.83
	1967	4	4	3	3	89.2	54.1	50.6	48.3	51.0	0.71	19.7	10.6	0.09	0.46	0.49	0.59
	1969	9	1	3	1	79.8	45.6	30.5	25	40.4	0.8	2.7	22.4	0.11	0.78	0.81	0.89
	1975	11	1	1	2	57.6	6.1	27.4	15.6	35.0	17.2	16.4	9.7	0.15	0.84	0.79	0.85
	1977	5	1	3	1	24.9	44.5	22.4	2.4	14.1	64.8	22.4	12.8	0.59	0.39	0.78	0.90
	1993	6	1	1	0	82.4	35.5	33.6	13.6	47.3	9.4	30.2	10.0	0.20	0.85	0.75	0.89
	1998	2	1	2	0	74.9	55.3	57.1	55.0	40.6	32.8	12.4	32.1	0.34	0.62	0.65	0.67
Validation	1984	1	1	2	1	29.5	29.2	35.3	25.2	56.5	61.7.	13.1	5.3	0.49	0.47	0.50	0.71
	2005	4	5	5	4	74.5	13.2	21.9	7.1	62.4	9.1	22.5	2.3	0.06	0.41	0.40	0.69
	2009	6	1	2	0	82.3	55.5	29.0	15.6	46.0	9.5	19.1	12.0	0.21	0.77	0.79	0.88
	2013	2	1	3	0	74.8	55.2	67.1	55.0	40.5	33.0	54.2	34.1	0.35	0.62	0.56	0.71
Average value		4.9	1.5	2.7	1.2	61.3	38.5	36.3	23.7	40.6	24.8	20.9	15.4	0.31	0.64	0.67	0.79

In the study area, the average value of the NSE of the widely-used Xin'anjiang model was as low as 0.31, and the average value of the error for flood peak time was 4.9 h. The average relative error of the runoff depth was 40.6%, which was nearly double the maximum error allowed by the Reservoir Administration Bureau of Liaoning Province (20%) [63]. The relative errors of flood peak discharge were all higher than 20%, and the average value exceeded the allowable error (20%) by almost double. Based on the above statistical results, the Xin'anjiang model demonstrated very low simulation performance in the research basin, could not reach the C-level simulation efficiency stipulated by the Reservoir Administration Bureau of Liaoning Province [63], and showed poor applicability in the study area. Compared with the Xin'anjiang model, the simulation efficiencies of the Liaoning unsaturated model and the original DHF model were somewhat improved, as the NSE and three errors were, to a certain extent, better. However, as Table 4 shows, the relative error for most floods in the study basin was still high and could not meet the actual forecast requirements by the Reservoir Administration Bureau of Liaoning Province [63]. The improved DHF model considering the influence of the upstream reservoirs showed better simulation results: the mean value of the NSE reached 0.79, the error of flood peak time was significantly reduced, the mean value of the relative error of runoff depth was 15.4%, and the relative error of flood peak discharge was close to the allowable error.

In comparison to the previous three models, the improved DHF model considering the influence of the upstream reservoirs showed the best efficiency.

Figures 4–6 illustrate three flood hydrographs simulated by four hydrological models in the Raoyang River, 1962, 1963, and 1984, respectively.

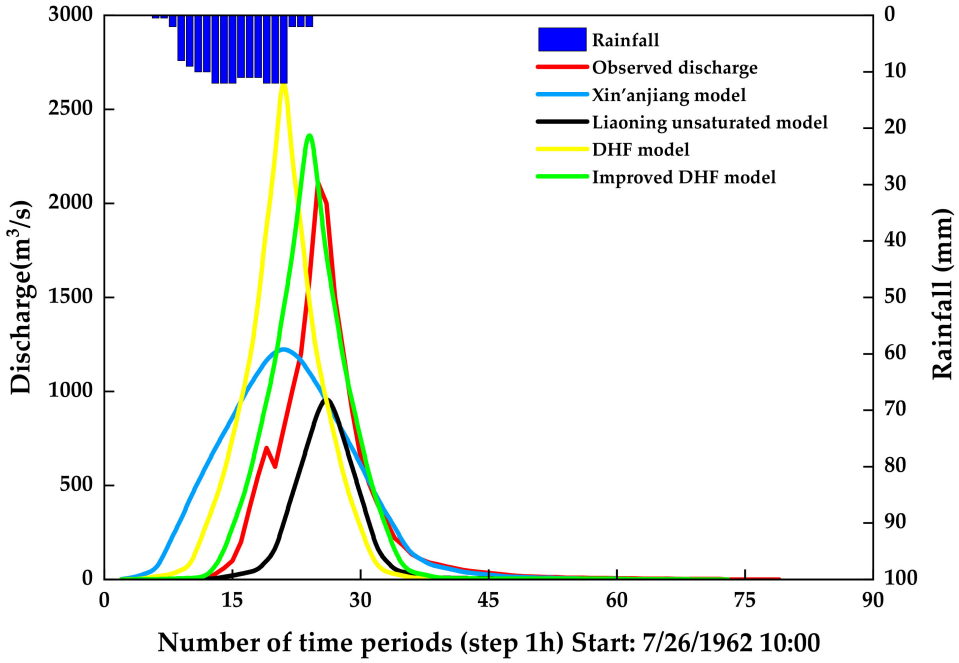

Figure 4. Flood hydrograph simulated by four hydrological models in 1962.

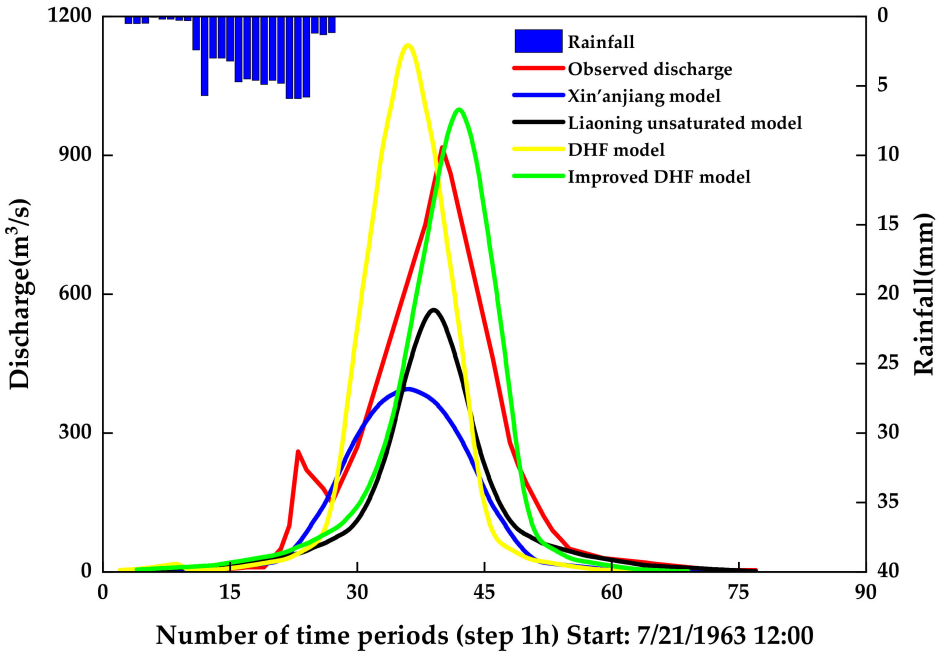

Figure 5. Flood hydrograph simulated by four hydrological models in 1963.

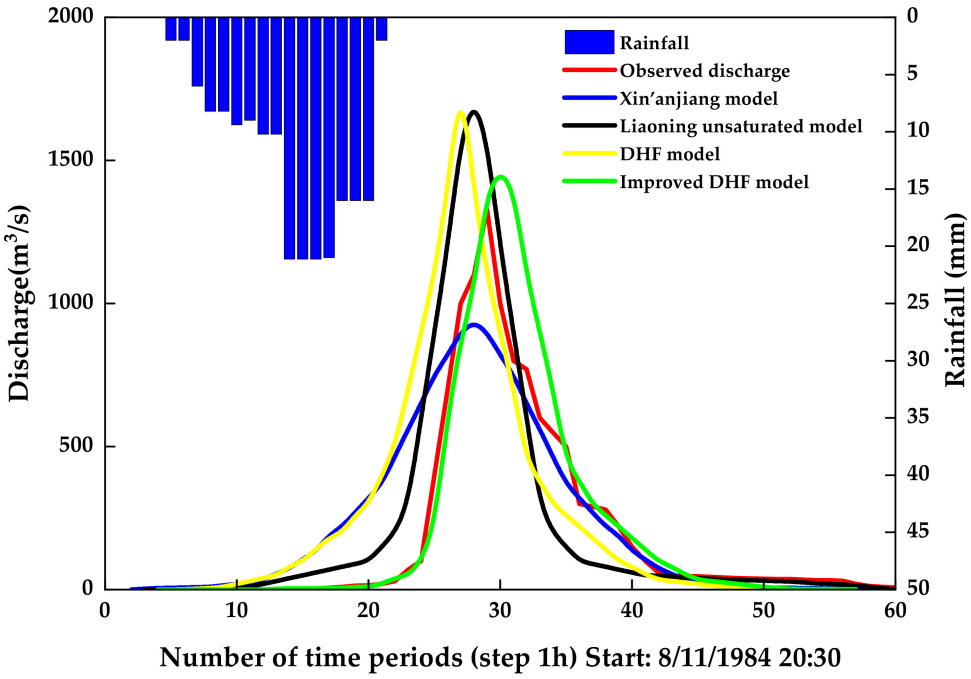

Figure 6. Flood hydrograph simulated by four hydrological models in 1984.

Quite obviously, the predictions became far removed from the observed discharge in the flood simulations by the Xin'anjiang model and the Liaoning unsaturated model, and the calculated flood hydrographs had large errors. Moreover, for the flood shown in Figure 6, the flood hydrographs simulated by the original DHF model and the improved DHF model were highly similar to the measured process, but the flood peak discharge calculated by the original DHF model was too large and the flood hydrograph simulated by the improved DHF model was more consistent with reality.

3.2. Discussion

An experiment based on four hydrological models was carried out in the Dongbaichengzi station watershed in the upper reaches of the Raoyang River. In comparison to the Xin'anjiang model, the Liaoning unsaturated model, and the DHF model, the improved DHF model, which considers the influence of the upstream reservoirs, showed the best efficiency.

The large difference in the simulation results of the four hydrological models in the Dongbaichengzi station watershed in the upper reaches of the Raoyang River spurred further analysis to discover the reasons for these discrepancies. In the first place, the study area is located in western Liaoning Province, China, an arid and semi-arid region. The soil water storage capacity in this area is weak and cannot meet the ideal conditions for saturation–excess runoff. This finding agreed with other research (Guo et al., 2015; Bao et al., 1997; Jin et al., 2015) [25,33,35]. Thus, because the Xin'anjiang model is based on the watershed saturation–excess runoff theory, an accurate simulation efficiency is difficult to obtain. A similar conclusion was reached by Kan (2017) [23]. Secondly, although the Liaoning unsaturated model and DHF model in western Liaoning are based on runoff yield under excess infiltration, their simulation efficiencies were indeed better than that of the Xin'anjiang model. A similar conclusion was reached by Liu (2019) [39]. However, these models failed to consider the influence of the upstream reservoirs in the long-drought region and the flood peak discharge calculated by the original DHF model was too large, making it difficult for them to meet the prediction requirements of arid and semi-arid areas in western Liaoning. This finding seemed consistent with other research in this field [39,46]. The improved DHF model, which considers the impoundment and regulation of small- and medium-sized reservoirs in the upper reaches of the basin, showed the best efficiency in the

Dongbaichengzi station watershed in the upper reaches of the Raoyang River, China. This finding agreed with other research [41–44]. However, the flood hydrograph simulated by the improved DHF model does not accurately express the nonlinear relationship between rainfall and runoff in detail, suggesting the need for further study.

4. Conclusions

This study investigated the performance of the Xin'anjiang model, the Liaoning unsaturated model, the DHF model, and the improved DHF model in western Liaoning, China, by carrying out a comparative study using data from 13 floods in the Dongbaichengzi watershed of the Raoyang River. The results revealed the following:

(1) The Xin'anjiang model is based on the watershed saturation–excess runoff theory. Hence, the model showed poor performance in the Dongbaichengzi station watershed in the upper reaches of the Raoyang River, which is characterised by runoff yield under the excess infiltration mechanism.

(2) Although the Liaoning unsaturated model and the DHF model take into account the spatial differences in the infiltration rate of the watershed, they leave out the influence of small- and medium-sized reservoirs in the upper reaches of the arid and semi-arid watershed in western Liaoning. Although the simulation and forecasting efficiencies of these models were better than that of the Xin'anjiang model, the relative error of flood peak discharge and runoff depth for most floods was still higher than the maximum error allowed by the Reservoir Administration Bureau of Liaoning Province, presenting an obstacle to applying them in this basin.

(3) The improved DHF model, which considers the influence of the upstream reservoirs, adopts the hyperosmosis runoff mechanism, which comprehensively accounts for the impoundment and regulation effect of small- and medium-sized reservoirs in the upper reaches of the research basin. In terms of the value of the NSE in the calibration and validation periods, the improved DHF model had better performance in this arid and semi-arid catchment than the other models tested. Therefore, the improved DHF model can provide new auxiliary information for flood prevention decisions in this area.

(4) In the arid and semi-arid areas of western Liaoning, China, the influencing factors of the runoff yield and confluence are very complex. The improved DHF model has been initially applied to the hydrological project of Liaoning Province, China, and has realised the monitoring of floods in the Raoyang River Basin. In the future, additional in-depth research on the regulating effect of reservoirs should include the characteristics of reservoir flood discharge and terrain features. The findings from future studies will thus support ongoing improvement of the simulation efficiencies of hydrological models to reduce the threat of flooding and facilitate the sustainable development of human society.

Author Contributions: H.J. and X.R. designed the algorithm, wrote the paper, and performed experiments based on arid and semi-arid regions. X.L. participated in the experimental analysis and revised the manuscript. X.R. revised the manuscript. All authors have read and agreed to the published version of the manuscript.

Funding: This study was funded by the National Key Research and Development Program of China (Grant No. 2019YFC1804304), the National Natural Science Foundation of China (Grant No. 41771478), and the Fundamental Research Funds for the Central Universities (Grant No. 2019B02514).

Institutional Review Board Statement: Not applicable.

Informed Consent Statement: Not applicable.

Data Availability Statement: Not applicable.

Conflicts of Interest: The authors declare that the research was conducted in the absence of any commercial or financial relationships that could be construed as a potential conflict of interest.

References

1. Kong, F.; Sun, S.; Wang, Y. Comprehensive Understanding the Disaster-Causing Mechanism, Governance Dilemma and Targeted Countermeasures of Urban Pluvial Flooding in China. *Water* **2021**, *13*, 1762. [CrossRef]
2. Tariq, M.A.U.R.; Farooq, R.; van de Giesen, N. A Critical Review of Flood Risk Management and the Selection of Suitable Measures. *Appl. Sci.* **2020**, *10*, 8752. [CrossRef]
3. Dong, B.; Xia, J.; Zhou, M.; Li, Q.; Ahmadian, R.; Falconer, R.A. Integrated modeling of 2D urban surface and 1D sewer hydrodynamic processes and flood risk assessment of people and vehicles. *Sci. Total Environ.* **2022**, *827*, 154098. [CrossRef]
4. Xiaotao, C. Recent progress in flood management in china. *Irrig. Drain.* **2006**, *55*, S75–S82. [CrossRef]
5. Coulthard, T.J.; Frostick, L.E. The Hull floods of 2007: Implications for the governance and management of urban drainage systems. *J. Flood Risk Manag.* **2010**, *3*, 223–231. [CrossRef]
6. Xing, Y.; Chen, H.; Liang, Q.; Ma, X. Improving the performance of city-scale hydrodynamic flood modelling through a GIS-based DEM correction method. *Nat. Hazards* **2022**, 1–23. [CrossRef]
7. Zhang, Y.; Hong, Y.; Wang, X.; Gourley, J.J.; Xue, X.; Saharia, M.; Ni, G.; Wang, G.; Huang, Y.; Chen, S.; et al. Hydrometeorological Analysis and Remote Sensing of Extremes: Was the July 2012 Beijing Flood Event Detectable and Predictable by Global Satellite Observing and Global Weather Modeling Systems? *J. Hydrometeorol.* **2015**, *16*, 381–395. [CrossRef]
8. Noor, F.; Haq, S.; Rakib, M.; Ahmed, T.; Jamal, Z.; Siam, Z.S.; Hasan, R.T.; Adnan, M.S.G.; Dewan, A.; Rahman, R.M. Water Level Forecasting Using Spatiotemporal Attention-Based Long Short-Term Memory Network. *Water* **2022**, *14*, 612. [CrossRef]
9. Chen, B.; Shi, F.; Lin, T.; Shi, P.; Zheng, J. Intensive Versus Extensive Events? Insights from Cumulative Flood-Induced Mortality Over the Globe, 1976–2016. *Int. J. Disaster Risk Sci.* **2020**, *11*, 441–451. [CrossRef]
10. Apel, H.; Merz, B.; Thieken, A.H. Quantification of uncertainties in flood risk assessments. *Int. J. River Basin Manag.* **2008**, *6*, 149–162. [CrossRef]
11. Wang, J.; Wang, H.J.; HONG, Y. A high-resolution flood forecasting and monitoring system for China using satellite remote sensing data. *Chin. Sci. Bull.* **2016**, *61*, 518–528. [CrossRef]
12. Li, B.Q.; Liang, Z.M.; Chang, Q.R.; Zhou, W.; Wang, H.; Wang, J.; Hu, Y.M. On the Operational Flood Forecasting Practices Using Low-Quality Data Input of a Distributed Hydrological Model. *Sustainability* **2020**, *12*, 8268. [CrossRef]
13. Li, Y.; Wang, G.X.; Liu, C.J.; Lin, S.; Guan, M.H.; Zhao, X.T. Improving Runoff Simulation and Forecasting with Segmenting Delay of Baseflow from Fast Surface Flow in Montane High-Vegetation-Covered Catchments. *Water* **2021**, *13*, 196. [CrossRef]
14. Hassan, S.M.T.; Lubczynski, M.W.; Niswonger, R.G.; Su, Z. Surface–groundwater interactions in hard rocks in Sardon Catchment of western Spain: An integrated modeling approach. *J. Hydrol.* **2014**, *517*, 390–410. [CrossRef]
15. Yong, B.; Ren, L.L.; Chen, X.; Zhang, Y.; Zhang, W.C.; Fu, C.B.; Niu, G.Y. Development of a large-scale hydrological model TOPX and its coupling with regional integrated environment modeling system RIEMS. *Chin. J. Geophys.* **2009**, *52*, 1954–1965. [CrossRef]
16. Yang, X.; Zhou, J.Z.; Fang, W.; Wang, Y.R. An Ensemble Flow Forecast Method Based on Autoregressive Model and Hydrological Uncertainty Processer. *Water* **2020**, *12*, 3138. [CrossRef]
17. Zhao, Y.J.; Xie, Q.Y.; Lu, Y.; Hu, B.Q. Hydrologic Evaluation of TRMM Multisatellite Precipitation Analysis for Nanliu River Basin in Humid Southwestern China. *Sci. Rep.* **2017**, *7*, 2470. [CrossRef]
18. Hao, G.; Li, J.; Song, L.; Li, H.; Li, Z. Comparison between the TOPMODEL and the Xin'anjiang model and their application to rainfall runoff simulation in semi-humid regions. *Environ. Earth Sci.* **2018**, *77*, 279. [CrossRef]
19. Chen, H.; Nan, Z.T. Progress in the Study of Hydrological Model Selection. *J. Glaciol. Geocryol.* **2010**, *32*, 397–404.
20. Qureshi, S.; Koohpayma, J.; Firozjaei, M.K.; Kakroodi, A.A. Evaluation of Seasonal, Drought, and Wet Condition Effects on Performance of Satellite-Based Precipitation Data over Different Climatic Conditions in Iran. *Remote Sens.* **2022**, *14*, 76. [CrossRef]
21. Chen, Y.L.; Han, J.T. Problems on flood forecasting in the semi-arid region. *Adv. Water Sci.* **2003**, *14*, 612–616. [CrossRef]
22. Bafitlhile, T.M.; Li, Z. Applicability of ε-Support Vector Machine and Artificial Neural Network for Flood Forecasting in Humid, Semi-Humid and Semi-Arid Basins in China. *Water* **2019**, *11*, 85. [CrossRef]
23. Kan, G.; He, X.; Ding, L.; Li, J.; Liang, K.; Hong, Y. Study on Applicability of Conceptual Hydrological Models for Flood Forecasting in Humid, Semi-Humid Semi-Arid and Arid Basins in China. *Water* **2017**, *9*, 719. [CrossRef]
24. Li, Y.; Wu, Z.; He, H.; Lu, G. Deterministic and Probabilistic Evaluation of Sub-Seasonal Precipitation Forecasts at Various Spatiotemporal Scales over China during the Boreal Summer Monsoon. *Atmosphere* **2021**, *12*, 1049. [CrossRef]
25. Guo, B.; Li, W.; Guo, J.; Chen, C. Risk Assessment of Regional Irrigation Water Demand and Supply in an Arid Inland River Basin of Northwestern China. *Sustainability* **2015**, *7*, 12958–12973. [CrossRef]
26. Bhuiyan, H.A.K.M.; McNairn, H.; Powers, J.; Merzouki, A. Application of HEC-HMS in a Cold Region Watershed and Use of RADARSAT-2 Soil Moisture in Initializing the Model. *Hydrology* **2017**, *4*, 9. [CrossRef]
27. Sunwoo, W.; Choi, M. Robust Initial Wetness Condition Framework of an Event-Based Rainfall–Runoff Model Using Remotely Sensed Soil Moisture. *Water* **2017**, *9*, 77. [CrossRef]
28. Koch, F.; Schlenz, F.; Prasch, M.; Appel, F.; Ruf, T.; Mauser, W. Soil Moisture Retrieval Based on GPS Signal Strength Attenuation. *Water* **2016**, *8*, 276. [CrossRef]
29. Wang, X. Vapor Flow Resistance of Dry Soil Layer to Soil Water Evaporation in Arid Environment: An Overview. *Water* **2015**, *7*, 4552–4574. [CrossRef]
30. Li, H.; Bao, S.; Wang, X.; Lv, H. Storm Flood Characteristics and Identification of Periodicity for Flood-Causing Rainstorms in the Second Songhua River Basin. *Water* **2016**, *8*, 529. [CrossRef]

31. Li, B.; Liang, Z.; Zhang, J.; Chen, X.; Jiang, X.; Wang, J.; Hu, Y. Risk Analysis of Reservoir Flood Routing Calculation Based on Inflow Forecast Uncertainty. *Water* **2016**, *8*, 486. [CrossRef]
32. Pilgrim, D.H.; Chapman, T.G.; Doran, D.G. Problems of rainfall-runoff modelling in arid and semiarid regions. *Hydrol. Sci. J.* **1988**, *33*, 379–400. [CrossRef]
33. Bao, W.M.; Wang, C.L. Vertical Mixed Runoff Model and Its Application. *J. China Hydrol.* **1997**, 18–21. [CrossRef]
34. Luo, W.S.; Hu, C.Q.; Han, J.T. Research on a model of runoff yield reflecting excess infiltration and excess storage simultaneously. *J. Soil Water Conserv.* **1992**, 6–13.
35. Jin, H.; Liang, R.; Wang, Y.; Tumula, P. Flood-Runoff in Semi-Arid and Sub-Humid Regions, a Case Study: A Simulation of Jianghe Watershed in Northern China. *Water* **2015**, *7*, 5155–5172. [CrossRef]
36. Adamowski, J.; Sun, K. Development of a coupled wavelet transform and neural network method for flow forecasting of non-perennial rivers in semi-arid watersheds. *J. Hydrol.* **2010**, *390*, 85–91. [CrossRef]
37. Sharifi Garmdareh, E.; Vafakhah, M.; Eslamian, S.S. Regional flood frequency analysis using support vector regression in arid and semi-arid regions of Iran. *Hydrol. Sci. J.* **2018**, *63*, 426–440. [CrossRef]
38. Feng, K.P.; Hong, Y.; Tian, J.C.; Tang, G.Q.; Kan, G.Y.; Luo, X.Y. Evaluating runoff simulation of multi-source precipitation data in small watersheds. *Arid Land Geogr.* **2020**, *43*, 1179–1191. [CrossRef]
39. Liu, S.; Zhang, L.P.; She, D.X.; Wang, Q.; Hu, C.; Xia, J. Applicability of catchment hydrologic models in arid and semi-arid regions. *Eng. J. Wuhan Univ.* **2019**, *52*, 384–390. [CrossRef]
40. Huang, P.N.; Li, Z.J.; Chen, J.; Li, Q.L.; Yao, C. Event-based hydrological modeling for detecting dominant hydrological process and suitable model strategy for semi-arid catchments. *J. Hydrol.* **2016**, *542*, 292–303. [CrossRef]
41. Sawunyama, T.; Senzanje, A.; Mhizha, A. Estimation of small reservoir storage capacities in Limpopo River Basin using geographical information systems (GIS) and remotely sensed surface areas: Case of Mzingwane catchment. *Phys. Chem. Earth* **2006**, *31*, 935–943. [CrossRef]
42. Liebe, J.; van de Giesen, N.; Andreini, M. Estimation of small reservoir storage capacities in a semi-arid environment A case study in the Upper East Region of Ghana. *Phys. Chem. Earth* **2005**, *30*, 448–454. [CrossRef]
43. Wu, J.; Liu, Z.; Yao, H.; Chen, X.; Chen, X.; Zheng, Y.; He, Y. Impacts of reservoir operations on multi-scale correlations between hydrological drought and meteorological drought. *J. Hydrol.* **2018**, *563*, 726–736. [CrossRef]
44. Yang, Z.-H.; Wang, J.; Liang, Z.-M.; Li, B.-Q.; Fu, Y.-P. Research on Flood Forecasting Method Considering the Influence of Small Reservoir with Missing Data. *China Rural Water Hydropower* **2021**, *3*, 98–102. [CrossRef]
45. Hu, C.; Xia, J.; She, D.X.; Yu, J.T.; Wang, F.D.; Sun, Y.H. The Application of Burr Distribution for Hydrological Frequency Analysis in Western Semi-arid Region of Liaoning Province. *J. China Hydrol.* **2019**, *39*, 20–26. [CrossRef]
46. Meng, Y. Grey relational analysis and multiple linear regression real-time flood forecasting model -Taking Dongbaichengzi Station in Raoyang River Basin as an example. *China Flood Drought Manag.* **2021**, *31*, 37–41. [CrossRef]
47. LI, J.N. Design low water for Wuzhou center port. *Port Waterw. Eng.* **2013**, *89–91*, 95. [CrossRef]
48. Committee, C. *Liaoning Hydrological Yearbook*; Liaoning Science and Techinology Publishing House: Shenyang, China, 2021.
49. Fei, Y.; Li, L.R.; Zhong, B.Y. Computation of Potential Evapotranspiration Using a Two-Source Method for the Xin'anjiang Hydrological Model. *J. Hydrol. Eng.* **2008**, *13*, 305–316.
50. Zang, S.H.; Li, Z.J.; Yao, C.; Zhang, K.; Sun, M.K.; Kong, X.Y. A New Runoff Routing Scheme for Xin'anjiang Model and Its Routing Parameters Estimation Based on Geographical Information. *Water* **2020**, *12*, 3429. [CrossRef]
51. Liu, J.T.; Song, H.Q.; Zhang, X.N.; Chen, X. A Discussion on Advances in Theories of Xinanjiang Model. *J. China Hydrol.* **2014**, *34*, 1–6. [CrossRef]
52. Li, H.X.; Zhang, Y.Q.; Chiew, F.H.S.; Xu, S.G. Predicting runoff in ungauged catchments by using Xinanjiang model with MODIS leaf area index. *J. Hydrol.* **2009**, *370*, 155–162. [CrossRef]
53. Shi, P.; Yang, T.; Xu, C.-Y.; Yong, B.; Huang, C.-S.; Li, Z.; Qin, Y.; Wang, X.; Zhou, X.; Li, S. Rainfall–Runoff Processes and Modelling in Regions Characterized by Deficiency in Soil Water Storage. *Water* **2019**, *11*, 1858. [CrossRef]
54. Chen, Z.C. Analysis and Research on the Applicability of Vertical Mixed Runoff Model in Western Liaoning. *Undergr. Water* **2019**, *41*, 168–170. [CrossRef]
55. Wang, M.; Peng, Y.; Liang, G. Application of DHF Model in Flood Forecasting for Shifosi Basin. *South North Water Transf. Water Sci. Technol.* **2012**, *10*, 93–97. [CrossRef]
56. Chiang, S.; Chang, C.H.; Chen, W.B. Comparison of Rainfall-Runoff Simulation between Support Vector Regression and HEC-HMS for a Rural Watershed in Taiwan. *Water* **2022**, *14*, 191. [CrossRef]
57. Dong, Q.J.; Cao, G.J.; Wang, X.J.; Dai, H.C.; Zhao, Y.F. Application prospect of PSO in hydrology. *Eng. Sci.* **2010**, *12*, 81–85. [CrossRef]
58. Liu, S.N.; Gan, H.; Wei, G.X. Application of PSO algorithm to calibrate the Xin'anjiang Hydrological Model. *J. Hydraul. Eng.* **2010**, *41*, 537–544.
59. Wang, K.; Zhang, L.J.; Zhang, L.L.; Cheng, S.J. Coupling Coordination Assessment on Sponge City Construction and Its Spatial Pattern in Henan Province, China. *Water* **2020**, *12*, 3482. [CrossRef]
60. Mariam, I.; Dalia, G.; Nesreen, G.; Kamel, G. Model-based multivariable regression model for thermal comfort in naturally ventilated spaces with personalized ventilation. *J. Build. Perform. Simul.* **2021**, *14*, 78–93. [CrossRef]

61. *GB/T 2482–2008*; Standard for Hydrological Information and Hydrological Forecasting; Standardization Administration of the People's Republic of China: Beijing, China, 2008; p. 16.
62. Moriasi, D.N.; Gitau, M.W.; Pai, N.; Daggupati, P. Hydrologic and Water Quality Models: Performance Measures and Evaluation Criteria. *Trans. ASABE* **2015**, *58*, 1763–1785. [CrossRef]
63. Lanlan, Y. Application of Dahuofang Model in Flood Forecasting of Small Watersheds in Eastern Liaoning Province. *Technol. Soil Water Conserv.* **2019**, *1*, 25–27. [CrossRef]